Electronic structure and possible martensitic transformation in Mn$_2$RhIn alloy

Z. REN[a], Y. LIU[a], S. LI[a*], X. ZHANG[a], G. LIU[b]

[a]*School of Mathematics and Physics, North China Electric Power University, Baoding 071003, P.R. China*
[b]*School of Material Science and Engineering, Hebei University of Technology, Tianjin 300130, P.R. China*

The electronic structure and the magnetic properties of Heusler alloy Mn$_2$RhIn have been studied using first-principles calculations. The phase transformation from the cubic structure to the tetragonal structure lowers the total energy effectively, indicating the possibility of a martensitic phase transition at low temperatures. With the tetragonal distortion, the minority DOS around the E_F splits into two peaks and the antibonding peak in minority spin moves to a lower energy. The E_F falls in a gap, reducing the value of N (E_F) effectively and increases the phase stability of the martensite.

1. Introduction

Since K. Ullakko *et al.*[1] reported the large magnetic-field-induced strains in the Ni$_2$MnGa alloy, the Mn-based Heusler alloys [2-4] have received considerable attentions for their potential application as ferromagnetic shape-memory alloys (FSMAs) in magnetic-field-controlled actuators and sensors. The FSMAs are magnetic materials that exhibit a martensitic transformation together with large magnetic-field-induced strains. The alloys have not only large strains but also high response frequencies because the shape memory effect can be controlled by applying magnetic field in addition to conventional controls by temperature and stress.

Until now, the most FSMAs among the Heusler alloys are the Ni-Mn based alloys, and the Ni-Mn-Z (Z=Ga, In, Fe, Al, Sn) [5-9] alloys have been predicted to be FSMAs by theoretical studies and confirmed by experimental investigations. And then, the Co-Ni-Ga alloys become an alternative to Ni-Mn-Ga shape memory alloys because they possess excellent low-temperature conventional shape memory properties and strong potential as high-temperature shape memory alloys [10-12], due to their wide stress and temperature stability ranges [13], high melting temperatures, good oxidation resistance, and cyclic stability [14]. Moreover, the Mn$_2$-based Heusler alloys exhibiting shape memory effect has been reported by Liu *et al.*[15]The magnetic-field-controlled effect creates a total strain up to 4.0% and changes the sign of the shape deformation effectively in the Mn$_2$NiGa alloy. In recent years, a large number of Heusler alloys [16, 17] have been predicted to be the FSMAs. However, the Heusler alloys consisting of *4d* or *5d* elements are rarely reported.

In this paper, we studied the electronic structure and the magnetic properties of Mn$_2$RhIn alloy containing *4d* element by first-principles calculations. The possibility of the martensitic transformation behavior is predicted.

2. Computational methods

The electronic structure was calculated using the pseudopotential method with a plane-wave basis set based on density-functional theory [18, 19]. The interactions between the atomic core and the valence electrons are described by the ultrasoft pseudopotential [20]. The electronic exchange-correlation energy has been treated under the local-density approximation (LDA) [21, 22]. For all cases, a plane-wave basis set cut-off of 500 eV was used.A mesh of 12×12×12 k-points was employed for Brillouin zone integrations. These parameters ensured good convergence of the total energy. The convergence tolerance in the calculations was selected as 1.0×10^{-6} eV/atom. The calculations were performed based on the theoretical equilibrium lattice parameters.

3. Result and discussion

3.1 Electronic structure in austenitic and martensitic phase

As shown in Fig. 1, Heusler alloys have a stoichiometric composition of X$_2$YZ, where X and Y atoms are transition metal elements, and the Z atom is an atom of a main group element. The Heusler alloys have four interpenetrating face-center-cubic (fcc) lattice. The two possible structures in austenitic phase are: Hg$_2$CuTi-type and Cu$_2$MnAl-type structures. In the Hg$_2$CuTi-type structure, the X atoms occupy the A (0 0 0) and B (1/4 1/4 1/4) sites, and the Y atom enters the C (1/2 1/2 1/2) site,

with the D (3/4 3/4 3/4) site occupied by the Z atom in Wyckoff coordinates. However, in the Cu$_2$MnAl-type structure, the X atoms occupy the A and the C sites, and the Y atom enters the B site, with the Z atom occupying the D site. For *3d* transition-metal elements, the preference of transition-metal elements is determined by the number of their valence electrons. The elements with less electrons prefer to occupy the B sites, while the others prefer to enter the (A, C) sites [23]. In this paper, in order to study the Heusler alloy Mn$_2$RhIn containing *4d* electron, we investigated the site preference before studying the magnetic properties and possible martensitic transformation.
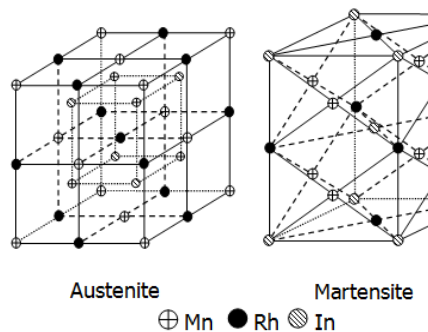

Fig. 1. The austenite and martensite structures for Mn$_2$RhIn alloys. As an example, Hg$_2$CuTi-type structure is shown for austenitic phase and tetragonal structure for martensitic phase

We investigated the electronic structure and made structure optimization on cubic austenitic Mn$_2$RhIn alloy in the Cu$_2$MnAl-type and the Hg$_2$CuTi-type structures by using first principle calculations. For both the paramagnetic (PM) and the ferromagnetic states, the coupling of Mn atoms were considered in calculations. In Fig. 2, the calculated total energy for Mn$_2$RhInare showed as a function of the lattice parameters for both the Cu$_2$MnAl-type and the Hg$_2$CuTi-type structures in the non-magnetic (PM) and the ferrimagnetic states. The zero of the energy has been chosen as the energy of the global equilibrium lattice constant. The equilibrium lattice constant of the austenitic Mn$_2$RhIn was derived by minimizing the total energy. As shown in Fig. 2, the calculated total energy for the Mn$_2$RhIn as a function of the lattice parameters for both the Cu$_2$MnAl-type and the Hg$_2$CuTi-type structures in the paramagnetic (PM) and ferrimagnetic states. In the two structures above, the ferrimagnetic states are more stable than the PM states because the ferrimagnetic states have lower energy. The energy difference between the Hg$_2$CuTi-type and the Cu$_2$MnAl-type structures is -0.48eV and thus the Mn$_2$RhIn alloy prefers to form the Hg$_2$CuTi-type structure, in line with the case of site preference for *3d* transition metal elements [24]. Thus the Mn$_2$RhIn alloy of Hg$_2$CuTi-type structure in ferrimagnetic state was considered as the model in the following investigations. The equilibrium lattice constant ofMn$_2$RhIn is 6.10Å, which is larger than

that of Mn$_2$NiAl [17], due to the larger atomic radii of Rh and In atoms compared with those of Ni and Al atoms.
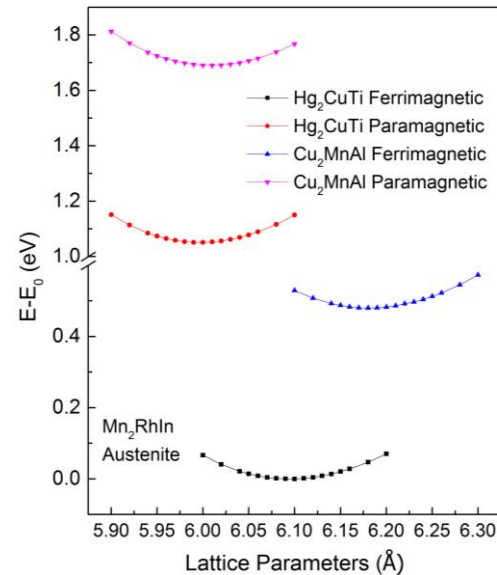

Fig. 2. Calculated total energy for Mn$_2$RhIn as a function of the lattice parameters for both the Cu$_2$MnAl- and the Hg$_2$CuTi-type of structure in the paramagnetic (PM) and ferrimagnetic states. The zero of the energy has been chosen as the energy of the global equilibrium lattice constant.
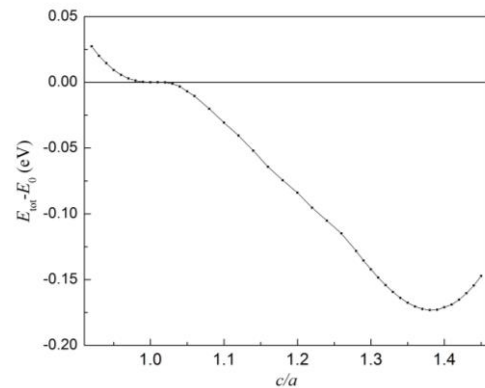

Fig. 3. Total energy as a function of the c/a ratio for Mn$_2$RhIn in the martensitic phase

The structural phase transition is nearly volume conserving [18, 24], which is a characteristic of the shape memory alloys. Similar results have been observed in many FSMAs, such as Mn$_2$NiZ (Z=Al, Ga, In) [25, 26]. In the optimization of the martensitic phase, we assumed no volume difference of the austenitic phase and the martensitic phase for convenience. Fig. 3 shows the calculated total energy as a function of the *c/a* ratio for Mn$_2$RhIn alloy in the martensitic phase, and the zero of total energy E_{tot} is the one in austenitic phase. The two local energy minima in the E_{tot}-*c/a* curve are: a very

shallow one at c/a =1.00 (austenite phase) and a deep one at c/a=1.38. Around c/a =1.00, with a very small tetragonal distortion, the energy of Mn$_2$RhIn changes little. The energy from c/a=0.95 to 1.05 keeps nearly constant, thus the c/a=1.00 is a metastable minima. The lowest energy in the whole curve is at c/a=1.38, meaning the most stable energy. Thus in the possible martensitic transformation, the c-axis lattice will expand and a, b-axis lattices will contract. The corresponding equilibrium lattice constants for martensite Mn$_2$RhIn are a=b=5.479Å and c=7.561Å, as listed in Table 1. As an example, the austenitic and the martensitic structures of the Mn$_2$RhIn alloy was presented in Fig. 1. The total energy difference between the martensitic and the austenitic phase is - 0.17eV/cell, indicating that the tetragonal phase is more stable and that a martensitic transformation may occur at the lowering temperature.

3.2 DOS and PDOS in austenitic and martensitic phase

The calculated total and partial densities of states (DOSs) of Mn$_2$RhIn in the austenitic and martensitic phases are shown in Fig. 4. In these figures, we chose the majority-spin states as positive value and the minority-spin states as negative value. In both austenitic phase and martensitic phase, the states between -6 eV and -4eV are mainly from the p electrons of In atoms in the occupied valence states, which hybridize with the d electrons of Rh atoms at the C sites. The total DOSs from -4 eV to +2 eV arise from d states of transition metal atoms. The widely spread d states are mainly from covalent hybridization between Mn and Rh atoms. In the majority-spin states, the bonding peaks around -3.5eV for austenite and martensite are mainly from covalent hybridization between Mn (B) and Rh (C) atoms; the anti-bonding peaks at 0.5eV are from Mn atoms at A sites. It is reported that the covalent hybridization between the lower-energy d states of the higher-valence transition metal atom like Rh and the higher-energy d states of the lower-valence transition metal atom like Mn can be strong and lead to the formation of bonding and antibonding bands [27].

For the austenitic phase, a two-peak structure in the minority-spin states is separated by an energy gap around the E_F. In the total DOS of austeniticMn$_2$RhIn, the E_F is located at the shoulder of a DOS peak in minority-spin and minority-spin directions, resulting in a relatively high N(E_F), which is the DOS at the Femi level. It is well known that a high N(E_F) will reduce the structure stability while low N(E_F) has the opposite effect [28, 29]. The PDOS of Mn (A) and Mn (B) contribute to both the bonding and antibonding parts in the total DOS. Mn atoms show the spin splitting in Mn (A) and Mn (B) sites, the Mn (A) peaks of majority and minority states appear above and below the E_F, respectively. However, the majority and minority peaks of Mn atom at B site arise below and above E_F, respectively.
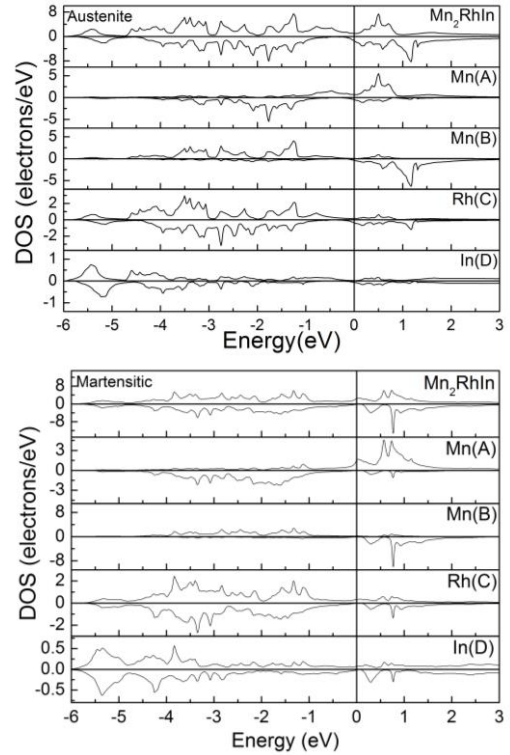

Fig. 4. The calculated total and partial density of states (DOS) of Mn$_2$RhIn in austenitic and martensitic phases.

In the martensitic phase, the tetragonal distortion does not affect the general shape of the total majority-spin states. The main change is that the anti-bonding peak in minority spin moves to a lower energy, and the E_F falls in a gap, reducing the value of N (E_F) effectively. In order to investigate the influence of tetragonal distortion, the calculated total DOS of Mn$_2$RhIn for c/a=0.96~1.40 is shown in Fig. 5, and the insets show the enlargement around the E_F. The shape of total DOS around the E_F remains substantially unchanged in the range of c/a=0.96~1.04, and the energy around c/a=1.00 changes little. For c/a=1.06~1.14, the minority-spin state DOS around the E_F splits into two peaks and E_F locates between the two peaks. From c/a=1.20 to 1.40, the minority DOS moves to the lower energy. In the martensitic phase, E_F moves to the bottom of the valley in the minority-spin states, reducing the value of N(E_F) effectively. Generally, the Jahn–Teller effect is an effect of removing the orbital and electronic degeneracies and lowering the overall energy. In DOS spectra, Jahn–Teller effect shows that the peak at the E_F in austenitic phase is divided into two peaks below and above the E_F with tetragonal distortion [30]. In Fig. 5 the DOSs of Mn$_2$RhIn at c/a=1.00 and c/a =1.38 shows the splitting peaks at the E_F, resulting in a lowering of the total energy and causing the martensitic transformation. The total DOS also decreases as increasing of c/a in Fig. 5, caused by the tetragonal distortion. These indicate that the tetragonal phase is more stable and that a martensitic transformation may occur at lowering temperature.
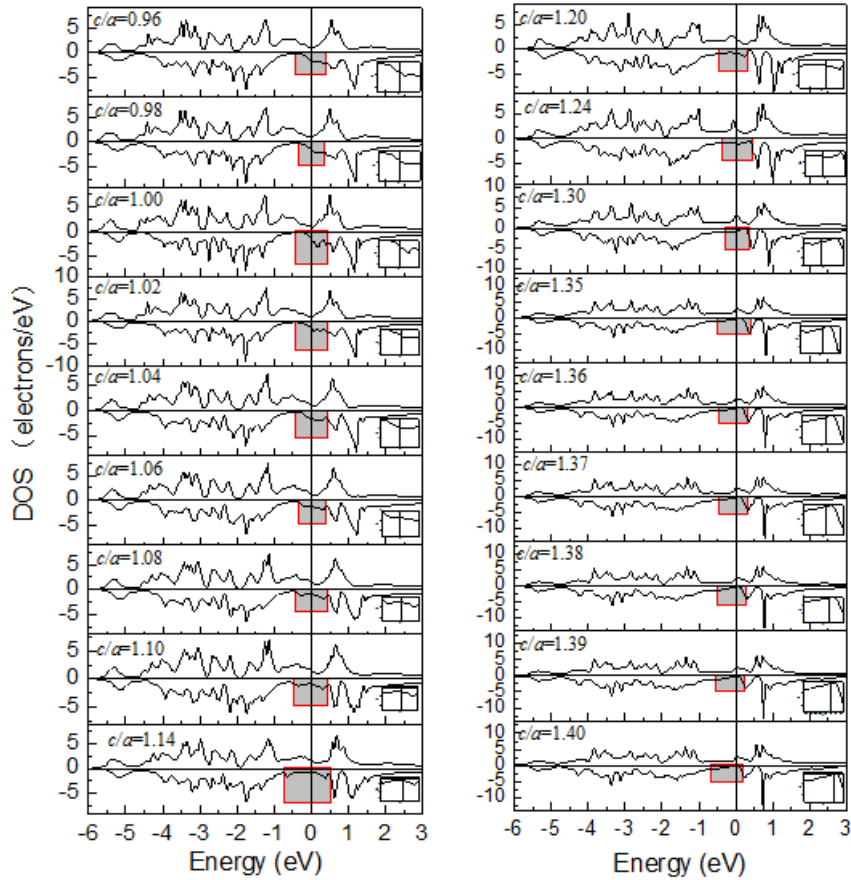
Fig. 5. The calculated total DOS of Mn$_2$RhIn for c/a=0.96~1.40

3.3 Magnetic properties

Generally, the magnetic moment is determined by the spin asymmetry of total number of electrons [31]. In Fig. 4, the total DOSs in majority-spin and minority-spin states are asymmetry, so the Mn$_2$RhIn alloy has magnetism in both austenitic phase and martensitic phase. The PDOSs of Mn atoms at A and B sites split in opposite directions, caused by the anti-parallel aligned spin moments of Mn (A) and Mn (B) atoms. The PDOS of Rh atom has a better symmetry and the spin moment of Rh atom is smaller than that of Mn atoms. The moments of In atoms for austenite and martensite are 0.04μ_B and 0μ_B, respectively. The calculated magnetic moments for austenitic and martensitic Mn$_2$RhIn are listed in Table 1. The Mn$_2$RhIn is a ferrimagnetic material, determined by the parallel aligned Rh and In atoms spin moments.

Table 1. The calculated lattice parameters a, b, c and magnetic moments for austenitic and martensitic Mn$_2$RhIn

Structure	a (Å)	b (Å)	c (Å)	c/a	M_{total} (μ_B)	$M_{\text{Mn(A)}}$ (μ_B)	$M_{\text{Mn(B)}}$ (μ_B)	$M_{\text{Rh(C)}}$ (μ_B)	$M_{\text{In(D)}}$ (μ_B)
Austenite	6.10	6.10	6.10	1.00	1.61	-2.64	3.84	0.38	0.04
Martensite	5.479	5.479	7.561	1.38	0.11	-3.50	3.58	0.02	0.00

In Fig. 4, with the tetragonal distortion, the majority antibonding peak at 0.50eV in the austenitic phase is shifted to 0.74eV in the martensitic phase. The variation of the total DOS indicates a charge transferring from the occupied to the unoccupied states. On the contrary, the minority antibonding peak at 1.17eV in the austenitic phase moves to 0.78eV in the martensitic phase, indicating charges transfer from the unoccupied to the occupied states. It is reported that the total magnetic moment is just the difference between the number of the occupied states

in majority spin and the unoccupied states in minority spin [32]. So the total spin moment of the martensitic phase is smaller than that of the austenitic phase. The calculated total and partial spin moments of the Mn_2RhIn are listed in Table 1.

The general configurations of PDOSs of the Mn (A) and the Mn (B) atoms do not change with the martensitic phase transformation. As a result, the spin moments of the Mn (A) and the Mn (B) atoms are also antiparallel, just like the discussed above in the austenite phase. The martensitic transformation makes the bonding peak in majority–spin state of Mn (A) move to a higher energy. For Mn (A) atom, the E_F just is located at the bonding peak. In the phase transition from austenite to martensite, the Mn (A) spin moment increases from -2.64 to $-3.50\mu_B$, mainly resulting in the decrease of total spin moment. Meanwhile, there are also contributions from other atoms. For example, the bonding peak in minority of Mn (B) moves left, decreasing the spin moment from 3.84 to $3.58\mu_B$. The total spin moments are 1.61 and $0.11\mu_B$ for the austenite and martensite, respectively.

The moment of the Mn_2RhIn alloy with martensitic phase is determined by the partial moments of Mn (A, B) and Rh (C) atoms. In Fig. 6, we presented the variations of the total and partial spin moments of Mn_2RhIn as functions of c/a ratio. The total moment around $c/a =1.00$ changes a little, corresponding to the metastable structure of the austenite. For the part of $c/a>1$, the total moment decreases with the c/a ratio increasing, due to the trend of increasing for the Mn (A, B) and Rh (C)atoms spin moments. The possible martensite phase appears at the point of $c/a =1.38$ and the moment is smaller than that of austenite of the Mn_2RhIn alloy. The spin moments of Mn (A) and Mn (B) atom keep anti-parallel aligned throughout the tetragonal distortional process and the system of Mn_2RhIn alloy shows ferrimagnetism.
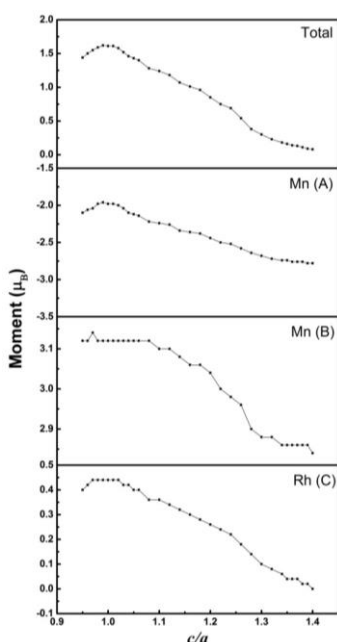

Fig. 6. Total and partial spin moments as functions of the c/a ratio for Mn₂RhIn.

4. Conclusion

The electronic structure and the magnetic properties of the Heusler alloy Mn_2RhIn have been studied theoretically. We investigated the electronic structure and made structure optimization on cubic austenitic Mn_2RhIn alloy in Cu_2MnAl-type and the Hg_2CuTi-type structures by using first principle calculations. Both paramagnetic (PM) and ferrimagnetic couplings between Mn atoms were considered in calculations. In the austenitic phase, the Mn_2RhIn of Hg_2CuTi-type structure in ferrimagnetic state is more stable than that of Cu_2MnAl-typestructure. The equilibrium lattice constant is 6.10Å. In tetragonal phase, the global energy minimum occurs at $c/a=1.38$. The corresponding equilibrium lattice constants for martensite Mn_2RhIn are $a=b=5.479$Å and $c=7.561$Å, respectively. The energy difference is 0.17eV/cell between the martensitic and the austenitic phases. The minority state DOS around the E_F splits into two peaks and E_F locates in the two peaks for the c/a ratio from 1.06 to 1.14. And in the range of $c/a=1.2\sim1.4$, the minority DOS moves to the lower energy. In the martensitic phase, the E_F moves to the bottom of the valley in the minority, reducing the value of $N(E_F)$ effectively. The calculated results indicate that the tetragonal phase is more stable and that a martensitic transformation may occur at lowering temperature. Both the austenitic and the martensitic phases are ferrimagnets, in which the partial moments of the Mn and the Rh atoms contribute most to the total moment. The spin moments of Mn (A) and Mn (B) atoms keep anti-parallel aligned in the tetragonal distortional process and the Mn_2RhIn alloy possesses ferrimagnetism.

References

[1] K. Ullakko, J. K. Huang, C. Kantner, R. C. O'Handley, V. V. Kokorin, Appl. Phys. Lett. **69**, 1966 (1996).
[2] S. Wrumehl, H. C. Kandpal, G. H. Fecher, C. Felser, J. Phys: Condens. Matter **18**, 6171 (2006).
[3] R. Weht, W. E. Pickett, Phys. Rev. B **60**, 13006 (1999).
[4] G. D. Liu, X. F. Dai, H. Y. Liu, J. L. Chen, Y. X. Li, G. Xiao, G. H. Wu, Phys. Rev. B **77**, 014424 (2008).
[5] V. V. Martynov, V. V. Kokorin, J Phys Ⅲ France **2**, 739 (1992).
[6] T. Tayama, T. Sakakibara, H. Sugawara, H. Sato, J. Magn. Magn. Mat. **310**, 2761 (2007).

[7] Z. H. Liu, M. Zhang, Y. T. Cui, Y. Q. Zhou, W. H. Wang, G. H. Wu, X. X. Zhang, G. Xiao, Appl. Phys. Lett. **82**, 424 (2003).

[8] A. Fujita, K. Fukamichi, F. Gejima, R. Kainuma, K. Isshida, Appl. Phys. Lett. **77**, 3054 (2001).

[9] Y. Sutou, Y. Imano, N. Koeda, T. Omori, R. Kainuma, K. Ishid, K. Oikawa, Appl. Phys. Lett. **85**, 4358 (2004).

[10] Y. X. Li, H. Y. Liu, F. B. Meng, L. Q. Yan, G. D. Liu, X. F. Dai, M. Zhang, Z. H. Liu, J. L. Chen, G. H. Wu, Appl. Phys. Lett. **84**, 3594 (2004).

[11] Y. Kishi, C. Craciunescu, M. Sato, T. Okazaki, Y. Furuya, M. Wutig, J. Magn. Magn. Mat. **262**, L186 (2003).

[12] R. Arróyave, A. Junkaew, A. Chivukula, S. Bajaj, C. Yao, A. Garay, Acta Materialia **58**, 5220 (2010).

[13] K. Oikawa, T. Ota, F. Gejima, T. Ohmori, R. Kainuma, K. Ishida, Mater Trans JIM **42**, 2472 (2001).

[14] J. Dadda, D. Canadinc, H. J. Maier, I. Karaman, H. E. Karaca, Y. I. Chumlyakov, Philos. Mag. **87**, 2313 (2007).

[15] G. D. Liu, J. L. Chen, Z. H. Liu, X. F. Dai, G. H. Wu, Appl. Phys. Lett. **87**, 262504 (2005).

[17] H. Luo, G. Liu, F. Meng, S. Li, W. Zhu, G. Wu, X. Zhu, C. Jiang, J. Physica B **405**, 3092 (2010).

[18] H. Z. Luo, F. B. Meng, G. D. Liu, H. Y. Liu, P. Z. Jia, E. K. Liu, W. H. Wang, G. H. Wu, Intermetallics **38**, 139 (2013).

[19] M. C. Payne, M. P. Teter, D. C. Allan, T. A. Arias, J. D. Joannopoulos, Rev. Mod. Phys. **64**, 1045 (1992).

[20] M. D. Segall, P. L. D. Lindan, M. J. Probert, C. J. Pickard, P. J. Hasnip, S. J. Clark, M. C. Payne, J. Phys.: Conden. Matt. **14**, 2717 (2002).

[21] D. Vanderbilt, Phys. Rev. B **41**, 7892 (1990).

[22] S. H. Vosko, L. Wilk, M. Nusair, Can. J. Phys. **58**, 1200 (1980).

[23] J. P. Perdew, A. Zunger, Phys. Rev. B **23**, 5048 (1981).

[24] H. C. Kandpal, G. H. Fecher, C. Felser, J. Phys.: D Appl. Phys. **40**, 1507 (2007).

[25] A. Chakrabarti, S. R. Barman, Appl. Phys. Lett. **94**, 161908 (2009).

[26] S. R. Barman, A. Chakrabarti, Phys. Rev. B **77**, 176401 (2008).

[27] S. Özdemir Kart, M. Uludoğan, I. Karaman, T. Çağın, Phys. Status Solid (a) **205**, 1026 (2008).

[28] I. Galanakis, P. H. Dederichs, N. Papanikolaou, Phys. Rev. B **66**, 134428 (2002).

[29] J. H. Xu, T. Oguchi, A. J. Freeman, Phys. Rev. B **36**, 4186 (1987).

[30] J. Tobola, J. Pierre, J. Alloys Compd. **296**, 243 (2000).

[31] S. Fujii, S. Ishida, S. Asano, J. Phys. Soc. Jpn. **58**, 3657 (1989).

[32] C. H. Park, B. C. Lee, J. I. Lee, J. Korean Phys. Soc. **47**, 655 (2005).

[33] I. Galanakis, P. H. Dederichs, Phy. Rev. B **66**, 134428 (2002).

_____

[*]Corresponding author: songtaoli2001@126.com